Research Article | Vol. 7, No. 10 | 1 Oct 2016 | BIOMEDICAL OPTICS EXPRESS 3905
Biomedical Optics EXPRESS

Evaluation of artifact reduction in optical coherence tomography angiography with real-time tracking and motion correction technology

ACNER CAMINO,[1] MIAO ZHANG,[1,2] SIMON S. GAO,[1] THOMAS S. HWANG,[1] UTKARSH SHARMA,[2] DAVID J. WILSON,[1] DAVID HUANG,[1] AND YALI JIA[1,*]

[1]*Casey Eye Institute, Oregon Health & Science University, Portland, OR, USA*
[2]*Optovue, Inc. 2800 Bayview Dr., Fremont, CA 94538, USA*
[*]*jiaya@ohsu.edu*

Abstract: Artifacts introduced by eye motion in optical coherence tomography angiography (OCTA) affect the interpretation of images and the quantification of parameters with clinical value. Eradication of such artifacts in OCTA remains a technical challenge. We developed an algorithm that recognizes five different types of motion artifacts and used it to evaluate the performance of three motion removal technologies. On *en face* maximum projection of flow images, the summed flow signal in each row and column and the correlation between neighboring rows and columns were calculated. Bright line artifacts were recognized by large summed flow signal. Drifts, distorted lines, and stretch artifacts exhibited abnormal correlation values. Residual lines were simultaneously a local maximum of summed flow and a local minimum of correlation. Tracking-assisted scanning integrated with motion correction technology (MCT) demonstrated higher performance than tracking or MCT alone in healthy and diabetic eyes.

OCIS codes: (170.4500) Optical coherence tomography; (170.4470) Ophthalmology; (100.2980) Image enhancement; (330.4150) Motion detection.

References and links

1. Y. Jia, O. Tan, J. Tokayer, B. Potsaid, Y. Wang, J. J. Liu, M. F. Kraus, H. Subhash, J. G. Fujimoto, J. Hornegger, and D. Huang, "Split-spectrum amplitude-decorrelation angiography with optical coherence tomography," Opt. Express **20**(4), 4710–4725 (2012).
2. R. K. Wang, S. L. Jacques, Z. Ma, S. Hurst, S. R. Hanson, and A. Gruber, "Three dimensional optical angiography," Opt. Express **15**(7), 4083–4097 (2007).
3. S. Makita, F. Jaillon, M. Yamanari, M. Miura, and Y. Yasuno, "Comprehensive in vivo micro-vascular imaging of the human eye by dual-beam-scan Doppler optical coherence angiography," Opt. Express **19**(2), 1271–1283 (2011).
4. S. Makita, Y. Hong, M. Yamanari, T. Yatagai, and Y. Yasuno, "Optical coherence angiography," Opt. Express **14**(17), 7821–7840 (2006).
5. T. S. Hwang, S. S. Gao, L. Liu, A. K. Lauer, S. T. Bailey, C. J. Flaxel, D. J. Wilson, D. Huang, and Y. Jia, "Automated quantification of capillary nonperfusion using optical coherence tomography angiography in diabetic retinopathy," JAMA Ophthalmol. **134**(4), 367–373 (2016).
6. Z. Chu, J. Lin, C. Gao, C. Xin, Q. Zhang, C.-L. Chen, L. Roisman, G. Gregori, P. J. Rosenfeld, and R. K. Wang, "Quantitative assessment of the retinal microvasculature using optical coherence tomography angiography," J. Biomed. Opt. **21**(6), 066008 (2016).
7. J. Conrath, R. Giorgi, D. Raccah, and B. Ridings, "Foveal avascular zone in diabetic retinopathy: quantitative vs qualitative assessment," Eye (Lond.) **19**(3), 322–326 (2005).
8. T. S. Hwang, Y. Jia, S. S. Gao, S. T. Bailey, A. K. Lauer, C. J. Flaxel, D. J. Wilson, and D. Huang, "Optical Coherence Tomography Angiography Features of Diabetic Retinopathy," Retina **35**(11), 2371–2376 (2015).
9. A. Ishibazawa, T. Nagaoka, A. Takahashi, T. Omae, T. Tani, K. Sogawa, H. Yokota, and A. Yoshida, "Optical Coherence Tomography Angiography in Diabetic Retinopathy: A Prospective Pilot Study," Am. J. Ophthalmol. **160**(1), 35–44 (2015).
10. Y. Jia, S. T. Bailey, D. J. Wilson, O. Tan, M. L. Klein, C. J. Flaxel, B. Potsaid, J. J. Liu, C. D. Lu, M. F. Kraus, J. G. Fujimoto, and D. Huang, "Quantitative optical coherence tomography angiography of choroidal neovascularization in age-related macular degeneration," Ophthalmology **121**(7), 1435–1444 (2014).

#270214 http://dx.doi.org/10.1364/BOE.7.003905
Journal © 2016 Received 8 Jul 2016; revised 26 Aug 2016; accepted 27 Aug 2016; published 6 Sep 2016

Biomedical Optics EXPRESS

11. N. V. Palejwala, Y. Jia, S. S. Gao, L. Liu, C. J. Flaxel, T. S. Hwang, A. K. Lauer, D. J. Wilson, D. Huang, and S. T. Bailey, "Detection of non-exudative choroidal neovascularization in age-related macular degeneration with optical coherence tomography angiography," Retina **35**(11), 2204–2211 (2015).
12. L. Kuehlewein, M. Bansal, T. L. Lenis, N. A. Iafe, S. R. Sadda, M. A. Bonini Filho, T. E. De Carlo, N. K. Waheed, J. S. Duker, and D. Sarraf, "Optical Coherence Tomography Angiography of Type 1 Neovascularization in Age-Related Macular Degeneration," Am. J. Ophthalmol. **160**(4), 739–748 (2015).
13. L. Kuehlewein, K. K. Dansingani, T. E. de Carlo, M. A. Bonini Filho, N. A. Iafe, T. L. Lenis, K. B. Freund, N. K. Waheed, J. S. Duker, S. R. Sadda, and D. Sarraf, "Optical Coherence Tomography Angiography of Type 3 Neovascularization Secondary to Age-Related Macular Degeneration," Retina **35**(11), 2229–2235 (2015).
14. Y. Jia, J. C. Morrison, J. Tokayer, O. Tan, L. Lombardi, B. Baumann, C. D. Lu, W. Choi, J. G. Fujimoto, and D. Huang, "Quantitative OCT angiography of optic nerve head blood flow," Biomed. Opt. Express **3**(12), 3127–3137 (2012).
15. Y. Jia, S. T. Bailey, T. S. Hwang, S. M. McClintic, S. S. Gao, M. E. Pennesi, C. J. Flaxel, A. K. Lauer, D. J. Wilson, J. Hornegger, J. G. Fujimoto, and D. Huang, "Quantitative optical coherence tomography angiography of vascular abnormalities in the living human eye," Proc. Natl. Acad. Sci. U.S.A. **112**(18), E2395–E2402 (2015).
16. Y. Jia, E. Wei, X. Wang, X. Zhang, J. C. Morrison, M. Parikh, L. H. Lombardi, D. M. Gattey, R. L. Armour, B. Edmunds, M. F. Kraus, J. G. Fujimoto, and D. Huang, "Optical coherence tomography angiography of optic disc perfusion in glaucoma," Ophthalmology **121**(7), 1322–1332 (2014).
17. L. Liu, Y. Jia, H. L. Takusagawa, A. D. Pechauer, B. Edmunds, L. Lombardi, E. Davis, J. C. Morrison, and D. Huang, "Optical Coherence Tomography Angiography of the Peripapillary Retina in Glaucoma," JAMA Ophthalmol. **133**(9), 1045–1052 (2015).
18. M. P. López-Sáez, E. Ordoqui, P. Tornero, A. Baeza, T. Sainza, J. M. Zubeldia, M. L. Baeza, and M. L. Baeza, "Fluorescein-induced allergic reaction," Ann. Allergy Asthma Immunol. **81**(5), 428–430 (1998).
19. S. Martinez-Conde, S. L. Macknik, and D. H. Hubel, "The role of fixational eye movements in visual perception," Nat. Rev. Neurosci. **5**(3), 229–240 (2004).
20. R. F. Spaide, J. G. Fujimoto, and N. K. Waheed, "Image Artifacts in Optical Coherence Tomography Angiography," Retina **35**(11), 2163–2180 (2015).
21. B. Lumbroso, D. Huang, C. Chen, Y. Jia, M. Rispoli, A. Romano, and N. Waheed, *Clinical OCT Angiography Atlas* (New Delhi, India: Jaypee Brothers Medical Publishers Ltd, 2015).
22. U. Sharma and M. J. Everett, "Improved data acquisition methods for reduced motion artifacts and applications in oct angiography," US Patent 8,857,988.
23. R. D. Ferguson, D. X. Hammer, L. A. Paunescu, S. Beaton, and J. S. Schuman, "Tracking optical coherence tomography," Opt. Lett. **29**(18), 2139–2141 (2004).
24. K. V. Vienola, B. Braaf, C. K. Sheehy, Q. Yang, P. Tiruveedhula, D. W. Arathorn, J. F. de Boer, and A. Roorda, "Real-time eye motion compensation for OCT imaging with tracking SLO," Biomed. Opt. Express **3**(11), 2950–2963 (2012).
25. B. Braaf, K. V. Vienola, C. K. Sheehy, Q. Yang, K. A. Vermeer, P. Tiruveedhula, D. W. Arathorn, A. Roorda, and J. F. de Boer, "Real-time eye motion correction in phase-resolved OCT angiography with tracking SLO," Biomed. Opt. Express **4**(1), 51–65 (2013).
26. Q. Zhang, Y. Huang, T. Zhang, S. Kubach, L. An, M. Laron, U. Sharma, and R. K. Wang, "Wide-field imaging of retinal vasculature using optical coherence tomography-based microangiography provided by motion tracking," J. Biomed. Opt. **20**(6), 066008 (2015).
27. C. K. Sheehy, Q. Yang, D. W. Arathorn, P. Tiruveedhula, J. F. de Boer, and A. Roorda, "High-speed, image-based eye tracking with a scanning laser ophthalmoscope," Biomed. Opt. Express **3**(10), 2611–2622 (2012).
28. M. F. Kraus, B. Potsaid, M. A. Mayer, R. Bock, B. Baumann, J. J. Liu, J. Hornegger, and J. G. Fujimoto, "Motion correction in optical coherence tomography volumes on a per A-scan basis using orthogonal scan patterns," Biomed. Opt. Express **3**(6), 1182–1199 (2012).
29. M. F. Kraus, J. J. Liu, J. Schottenhamml, C. L. Chen, A. Budai, L. Branchini, T. Ko, H. Ishikawa, G. Wollstein, J. Schuman, J. S. Duker, J. G. Fujimoto, and J. Hornegger, "Quantitative 3D-OCT motion correction with tilt and illumination correction, robust similarity measure and regularization," Biomed. Opt. Express **5**(8), 2591–2613 (2014).
30. J. C.-V. G. Staurenghi and J.-F. Korobelnik, "Optical Coherence Tomography Angiography of the Retinal Microvasculature using the Zeiss AngioPlex," European Ophthalmic Review **9**(02), 147 (2015).
31. P. Zang, G. Liu, M. Zhang, C. Dongye, J. Wang, A. D. Pechauer, T. S. Hwang, D. J. Wilson, D. Huang, D. Li, and Y. Jia, "Automated motion correction using parallel-strip registration for wide-field en face OCT angiogram," Biomed. Opt. Express **7**(7), 2823–2836 (2016).
32. A. Camino, M. Zhang, C. Dongye, A. D. Pechauer, T. S. Hwang, S. T. Bailey, B. Lujan, D. J. Wilson, D. Huang, and Y. Jia, "Automated registration and enhanced processing of clinical optical coherence tomography angiography," Quant. Imaging Med. Surg. **6**, 391–401 (2016).
33. T. H. Ko, X. Luo, Y. Zhao, and B. Jang, "Imaging with real-time tracking using optical coherence tomography," US Patent 20120274783.
34. M. Zhang, J. Wang, A. D. Pechauer, T. S. Hwang, S. S. Gao, L. Liu, L. Liu, S. T. Bailey, D. J. Wilson, D. Huang, and Y. Jia, "Advanced image processing for optical coherence tomographic angiography of macular diseases," Biomed. Opt. Express **6**(12), 4661–4675 (2015).

Biomedical Optics EXPRESS

35. K. Pearson, "Note on regression and inheritance in the case of two parents," Proc. R. Soc. Lond. **58**(-1), 240 (1895).
36. L. Chidambara, S. G. Gadde, N. K. Yadav, C. Jayadev, D. Bhanushali, A. M. Appaji, M. Akkali, A. Khurana, and R. Shetty, "Characteristics and quantification of vascular changes in macular telangiectasia type 2 on optical coherence tomography angiography," Br. J. Ophthalmol. **1136**, 307941 (2016).
37. W. A. Samara, A. Shahlaee, J. Sridhar, M. A. Khan, A. C. Ho, and J. Hsu, "Quantitative Optical Coherence Tomography Angiography Features and Visual Function in Eyes With Branch Retinal Vein Occlusion," Am. J. Ophthalmol. **166**, 76–83 (2016).

1. Introduction

Optical coherence tomography angiography (OCTA) is a novel, noninvasive technique that images the retinal and choroidal circulations [1–4]. Recently, the potential for OCTA in clinical evaluation has been demonstrated in vascular diseases such as diabetic retinopathy (DR) [5–9] age-related macular degeneration (AMD) [10–13] and glaucoma [14–17]. As OCTA uses the motion of blood cells as intrinsic contrast to identify vascular networks [15, 18], it avoids the need for intravenous dye injection. However, OCTA is sensitive to eye motion.

Artifacts produced by eye motion during scanning remain a technical challenge [19–21]. The split-spectrum amplitude-decorrelation angiography (SSADA) algorithm is tolerant to axial motion by reducing the resolution in the axial direction; however, transverse eye motion such as microsaccades introduce artifacts that manifest as bright lines or stripes on *en face* OCTA.

Two main approaches to eliminate this problem have been adopted in commercial systems. The Angioplex (Zeiss Meditec, Inc., Dublin, CA, USA) integrates a scanning laser ophthalmoscope (SLO) in a real-time eye tracking system that makes adjustments when motion is detected [22]. Tracking of the scanning optical coherence tomography (OCT) beam to compensate for eye motion was introduced over a decade ago [23]. Since then, scanning assisted by SLO has been successfully implemented in OCT [24] and OCTA [25, 26]. Motion correction bandwidth of 32 Hz and latency of 2.5 ms between detection and correction have been reported [24, 27]. Alternatively, the Avanti RTVue-XR OCT system (Optovue, Inc. Fremont, CA, USA) utilizes motion correction technology (MCT), an algorithm based on the registration of two OCT volumes acquired with orthogonal scanning axes [28, 29]. Although hardware and software solutions greatly improve the scan quality, residual lines and distorted lines can persist after MCT [20] and evidence of motion is observed in SLO-assisted scanning [30]. While MCT performance is challenged by big saccadic motion, real-time tracking performance is often limited by the resolution of fundus image as well as the gradual loss of image quality caused by fatigue experienced by patients due to longer scanning times. The residual artifacts in either of these approaches reduce the repeatability and accuracy of quantitative studies based on OCTA. Although *en face* registration algorithms that considerably decrease the prevalence of residual artifacts have been demonstrated [31, 32], they are two-dimensional in nature or necessitate a larger number of scans [32].

Recently, the RTVue-XR system has incorporated a real-time eye tracking function based on the light intensity detected by an infrared (IR) full-field fundus camera. This tracking configuration is less difficult to implement than an SLO and simplifies laser safety considerations since it is based on uniform illumination of a large area instead of scanning of a focused beam. The combination of tracking-assisted scanning with MCT registration enables greater reduction of motion artifacts as it employs two levels of motion artifact removal. The first level, eye tracking based on IR image, performs real-time OCT scan correction to account for eye blinks, saccades, and fixation drifts. The second level, motion correction technology (MCT), is a post processing step that performs precise pixel level registration in three dimensions to further improve the motion correction accuracy and the resulting image quality. In this study, we have developed an automated motion artifact detection algorithm to assess its effectiveness for the suppression of artifacts in OCTA of healthy and diabetic retinopathy eyes.

Biomedical Optics EXPRESS

2. Methods

2.1 Study population

This study was conducted at the Casey Eye Institute of Oregon Health & Science University (OHSU). Ten healthy participants and 23 participants with DR were enrolled in the study. Written informed consent was obtained from all participants recruited. The protocol was approved by the Institutional Review Board/Ethics Committee of OHSU and adhered to the tenants of the Declaration of Helsinki in the treatment of human participants.

2.2 Data acquisition

OCTA imaging was performed with the Avanti RTVue-XR OCT system, operating at a central wavelength of 840 nm, a bandwidth of 45 nm, optical power of 0.65 mW and an A-scan rate of 70 kHz. The eye tracking system incorporated in the RTVue-XR relies on an IR video camera operating at 30 frames per second, a graphics processing unit for motion detection, and a module for error analysis [33]. The retina is uniformly illuminated by light from LED at a wavelength of 735 nm. Motion is identified by comparing current and stored fundus feature boundaries detected by the IR camera. An internal clock records the timing relationship between the OCT frame and the motion detected in the infrared video. The system detects blinking and saccadic motion greater than 60 μm and waits for the transient motion to finish. Once the eye has stabilized, the OCT beam is steered back to the beginning of the position where motion was previously registered and the system resumes data acquisition. It could take up to 33 ms to detect a motion event.

Each acquisition consisted of two scans at orthogonal raster directions. Each scan consisted of 608 B-frames, composed of a set of 304 A-lines acquired two times at each of the 304 raster positions. Acquisition of a 3×3 mm^2 scanning area without tracking took 2.9 seconds. Structural OCT data was obtained by averaging the OCT data of both frames acquired at the same raster position. The SSADA algorithm calculated OCTA data. This algorithm divides the OCT spectrum into eleven bands, computes the decorrelation between two B-scans at the same raster position, and finally averages the result obtained for all spectral bands.

In healthy participants, a single eye was imaged twice with tracking and twice without. For participants with DR, a single eye was imaged twice with either tracking turned on or off. We allowed participants to rest for a few seconds between acquisitions and asked them to maintain fixation on a target during the scanning, regardless of whether tracking was on or off. Participants with DR were allowed to blink during acquisitions with tracking. A signal strength index (SSI) that represents the scan's overall reflectance signal strength was calculated by the RTVue software. Data from three diabetic eyes was rejected due to low signal levels (SSI < 60). A total of 80 acquisitions were included for analysis, 40 for healthy eyes and 40 for diabetic eyes.

The two orthogonal scans (x-fast and y-fast) forming each acquisition were registered by the MCT software to build a single volumetric data set. MCT corrects motion by a mechanism that first finds an optimal objective function that estimates a 3D displacement vector for each A-scan [29]. The algorithm is capable of correcting tilts and changes in illumination. Volumes are merged by a scheme that attenuates small motion artifacts undetected by the tracking system and increases the signal-to-noise ratio (SNR) of the angiograms [28].

2.3 Data processing

A directional graph-search method developed by Zhang *et al*. [34] automatically segmented retinal layers in the structural OCT images. An expert grader examined the segmentation and manually corrected errors. Then, we generated an *en face* angiogram of the superficial plexus from the SSADA volume by projecting the maximum decorrelation value of the voxels

Biomedical Optics EXPRESS

between the inner limiting membrane and superficial half of the inner plexiform layer. The resulting 2D image, in which pixel amplitudes are SSADA decorrelation values, is exported to the artifact detection algorithm.

2.4 Image quality assessment

We assessed the performance of tracking only, MCT only, and tracking with MCT in eliminating bright line artifacts contained in the original scans (x-fast and y-fast). Bright line artifacts can be recognized in *en face* angiograms by computing the summation of the flow signal in rows or columns (S), as observed in Fig. 1(A). Artifactual lines in Fig. 1(B) contain summed flow signal above the threshold $S_{th} = \overline{S} + 2\sigma_S$, where $\overline{S}$ is the summed flow average and σ_S is the standard deviation.

In tracking-assisted scans, we were interested in assessing the fraction of frames where motion was detected and corrected by the tracking system. Since the tracking does not correct the eye drift after a saccade, the frames affected by motion could be recognized by computing the correlation (ρ) of adjacent rows or columns. On the j^{th} column, ρ is defined as:

$$\rho_j = \frac{1}{(N-1)} \sum_{i=1}^{N} \left(\frac{A_{i,j}\,\overline{A}_j}{\sigma_{A_j}} \times \frac{A_{i,j+1} - \overline{A}_{j+1}}{\sigma_{A_{j+1}}} \right) \tag{1}$$

where $\overline{A}_j$ is the average of the pixel amplitudes in a column j, σ_{A_j} is the standard deviation and N = 304. Rescanned frames that are affected by eye drift exhibit a correlation lower than the threshold $\rho_{th} = \overline{\rho} - 2\sigma_\rho$ (Fig. 1(C)-1(D)). Threshold values were identified empirically.

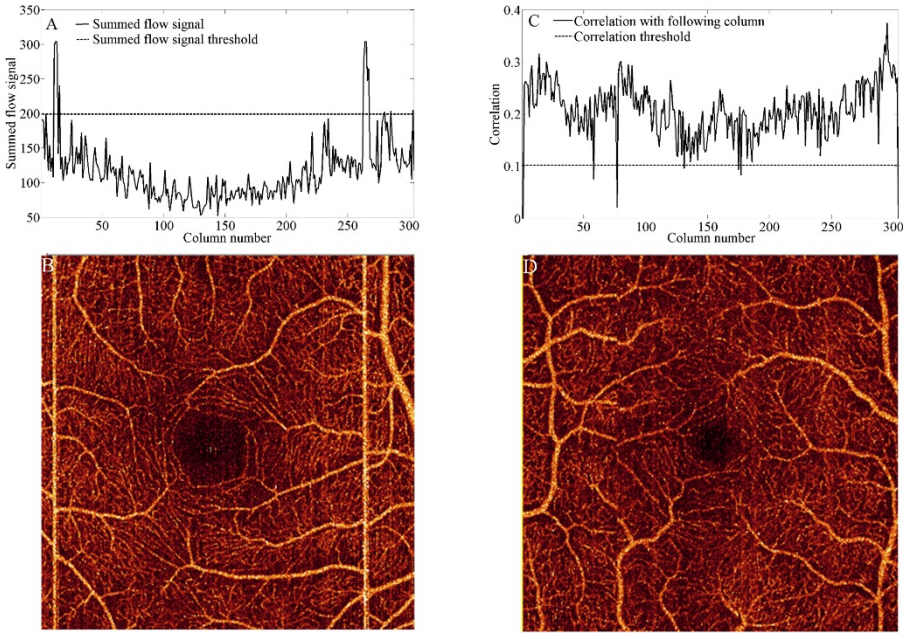

Fig. 1. Detection of motion artifacts in an x-fast or y-fast scan. (A) Bright line artifacts can be identified by setting a summed flow signal threshold. (B) *En face* angiogram obtained from a scan without tracking. (C) Drift artifacts can be identified by setting a correlation threshold. (D) *En face* angiogram obtained from a scan assisted by tracking.

Acquisitions processed by MCT or tracking plus MCT were assessed by computing the number of distorted lines, stretch artifacts, and residual lines remaining in *en face*

Biomedical Optics EXPRESS

angiograms. Interpolation errors cause distorted lines and stretch artifacts. Distorted lines appear at the position of eye motion in the event of microsaccades (Fig. 2(B), 2(B1)), exhibit abnormally low correlation values ($\rho_{Dist} < \overline{\rho} - 3\sigma_{\rho}$, Fig. 2(A)) and are usually found in stripes of more than one line width. Stretch artifacts (Fig. 2(B), 2(B2)) appear near the borders of the angiogram where the registered volumes did not overlap. Motion between x-fast or y-fast scans, not within a scan, cause stretch artifacts, which are recognized by abnormally high correlation values ($\rho_{Stretch} < \overline{\rho} + 2\sigma_{\rho}$, Fig. 2(A)).

Residual lines are continuous lines appearing where bright lines in the x-fast or y-fast scans were not completely removed by the weighted merging feature of MCT (Fig. 2(D), 2(D1), 2(D2) and 2(D5)). They are difficult to detect by simply imposing a threshold on their summed flow signal or correlation values, since vessels with a large vertical or horizontal section can be mistakenly identified. We identify lines that are simultaneously a local summed flow maximum and a local correlation minimum (Fig. 2(C)). Moreover, local extrema are only considered if they cross the correlation threshold ρ_{th} and summed flow signal threshold S_{th} defined above. In this manner, the software neglects lines that are only partially affected (Fig. 2(D), 2(D3) and 2(D6)). Column D4 is detected as a distorted line.

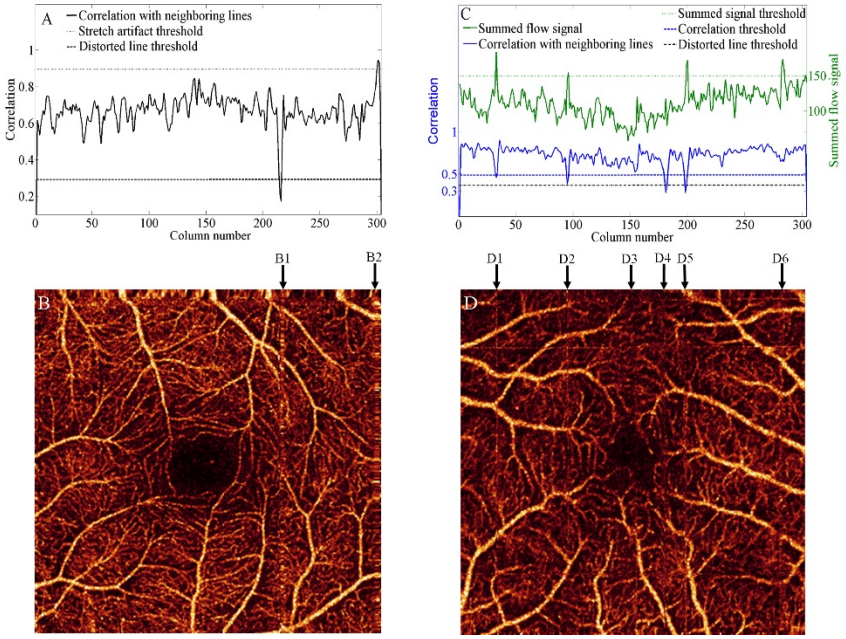

Fig. 2. Automated recognition of artifacts in acquisitions processed by MCT or tracking with MCT. The correlation with neighboring lines and thresholds considered for distorted stripes and stretch artifacts are shown in (A). An example of distorted stripe (B1) and stretch artifact (B2) that correspond to (A) are represented in (B). The correlation and summed flow signal thresholds considered for residual lines are shown in (C). Columns of interest (D1-D6) in the identification of residual lines are represented in (D).

Since motion artifacts contain a collection of pixels with abnormal signal intensity, inaccuracies can be introduced during quantification of clinically useful parameters. Therefore, we are interested in evaluating the similarity between the pair of scans obtained from each participant within a visit. The measurement of angiographic similarity can better reflect the scan repeatability affected by various motion artifacts. First, affine registration of the two superficial plexuses was performed. Then, the area common to both angiograms was cropped and Pearson's product-moment correlation coefficient (r) between the two matrices A and B was calculated by:

Biomedical Optics EXPRESS

$$r = \frac{\sum_{i=1}^{n}(A_i - \bar{A})(B_i - \bar{B})}{\sqrt{\sum_{i=1}^{n}(A_i - \bar{A})^2}\sqrt{\sum_{i=1}^{n}(B_i - \bar{B})^2}} \quad (2)$$

where n is the number of pixels in the cropped image. This coefficient takes values closer to 1 for strong positive correlation [35], indicating better similarity between angiograms A and B.

In all acquisition modes, the prevalence of artifacts (P) in *en face* angiograms with N rows and N columns is calculated as the proportion of artefactual rows (R) and columns (C) above artifact threshold values as:

$$P = \frac{R + C}{2N}. \quad (3)$$

A one-sample t-test evaluates the statistical significance of artifact prevalence changes in both tracking modes.

3. Results

First, we assessed the performance of the artifact recognition algorithm by comparing its results to those of a human grader. Sensitivity and specificity for the group of healthy participants are shown on Table 1. The algorithm performed at 100% sensitivity in detecting bright lines, distorted lines, and stretch artifacts. For subtle artifacts such as drifts and residual lines, sensitivity was above 92%. Specificity was above 99% for all types of artifacts, given the small number of false positive lines.

Table 1. Comparison of the number of artifacts detected by a human grader and the artifact recognition algorithm in healthy participants with tracking. Sensitivity and specificity of the algorithm.

Artifact type	Acquisition mode	Grader	Algorithm	Sensitivity	Specificity
Bright lines	x/y-fast & tracking off	0.020	0.021	100%	99.8%
Drift artifacts	x/y-fast & tracking on	0.0031	0.0029	94.1%	99.5%
Residual lines	tracking and MCT	0.0010	0.0010	92.3%	99.9%
Distorted lines	tracking and MCT	0.0005	0.0005	100%	100%
Stretch artifacts	tracking and MCT	0.0021	0.0023	100%	99.8%

The effect of tracking-assisted scans on the number of artifacts was evaluated on the healthy and diabetic groups. Figure 3 shows two x-fast scans of the same eye, with tracking (A1-B1) and without tracking (A2-B2). Black arrows in Fig. 3(B1) indicate drift artifacts at frames where microsaccadic motion occurred and no bright lines appeared. Tracking-assisted scanning reduced the prevalence of bright lines by a 42% in *en face* OCTA (Fig. 4) of the healthy group ($p < 0.05$) and by a 30% in the diabetic group ($p < 0.05$). However, as observed on structural OCT images (Figs. 3(A1)-3(A2)), the prevalence of eye motion is similar in both tracking modes. Consequently, although the total amount of artifacts (bright lines + drifts) was slightly reduced (Fig. 4), it was not statistically significant ($p > 0.05$).

Biomedical Optics EXPRESS

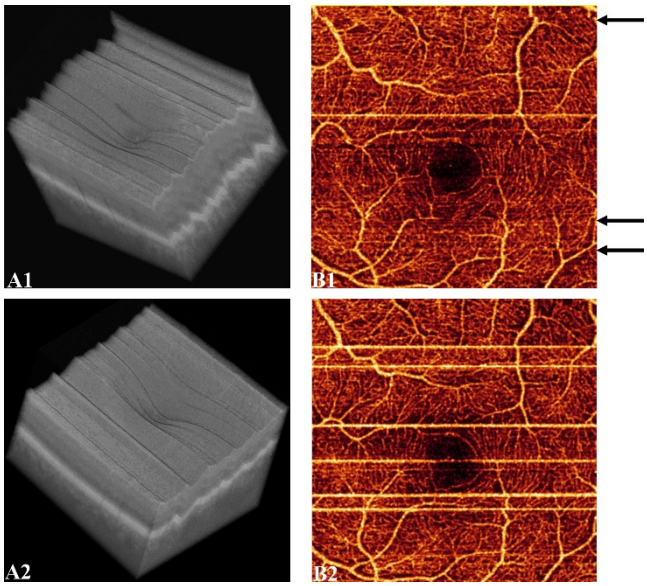

Fig. 3. X-fast scans of the same eye with (A1-B1) and without (A2-B2) tracking. Volumetric OCT images are represented in (A1-A2) and the corresponding *en face* OCTA of the superficial plexus in (B1-B2). Saccadic motion without manifestation of bright lines is indicated by black arrows in B1.

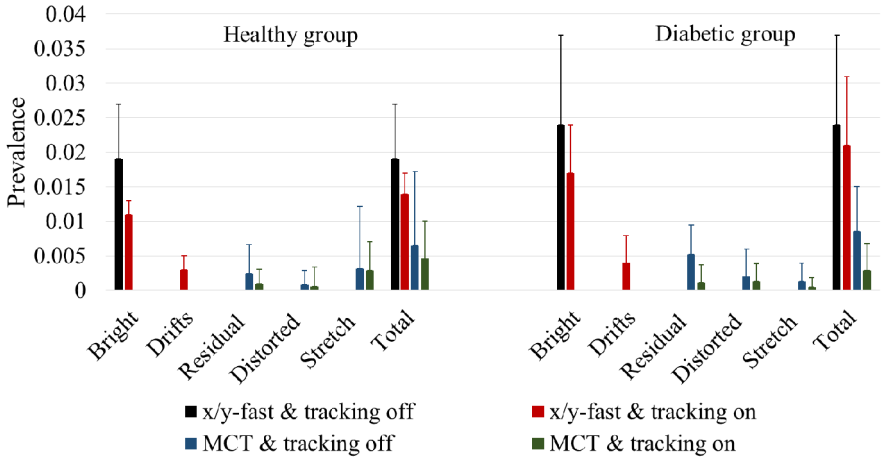

Fig. 4. Comparison of the average and standard deviation of artifact prevalence in x/y-fast scans without tracking, x/y-fast scans with tracking, MCT of scans acquired without tracking and MCT of tracking-assisted scans.

The efficacy of MCT in eliminating original artifacts was also studied. While all x/y-fast acquisitions contained at least one bright line, 25% of the MCT *en face* angiograms were completely free of artifacts in the healthy group and 10% in the diabetic group. Residual and distorted lines were more prevalent in the diabetic group than in the healthy group, as shown in Fig. 4. Although MCT did occasionally introduce an additional artifact (stretch), total artifact prevalence was reduced by a 65% in both the healthy ($p < 0.01$) and diabetic groups ($p < 0.05$).

Tracking integrated with MCT increased the proportion of *en face* angiograms completely free of artifacts to 55% in both groups. Seventy percent of the *en face* angiograms were free of residual lines, and 95% were free of distorted lines. Artifact prevalence was reduced by 76% in the healthy group and 88% in the diabetic group compared to x/y-fast acquisitions

Biomedical Optics EXPRESS

without tracking. This acquisition mode outperformed MCT only (Fig. 4) in reducing the total amount of artifacts in the healthy and diabetic groups ($p < 0.05$).

In terms of similarity between consecutive acquisitions, two angiograms obtained by tracking with MCT were more correlated than those acquired without tracking (0.75 ± 0.03 vs 0.72 ± 0.03, $p < 0.01$). The representative example in Fig. 5 shows the dissimilarity between two scans without tracking (Fig. 5(A1)-5(A2)), $r = 0.74$). In contrast, the pair of tracking-assisted scans showed improved similarity due to a visible reduction of artifacts (Fig. 5(B1)-5(B2)), $r = 0.77$). Visualization of vascular details was also improved in tracking with MCT (Fig. 5(B3)-5(B4)) compared to MCT only acquisitions (Fig. 5(A3)-5(A4)).

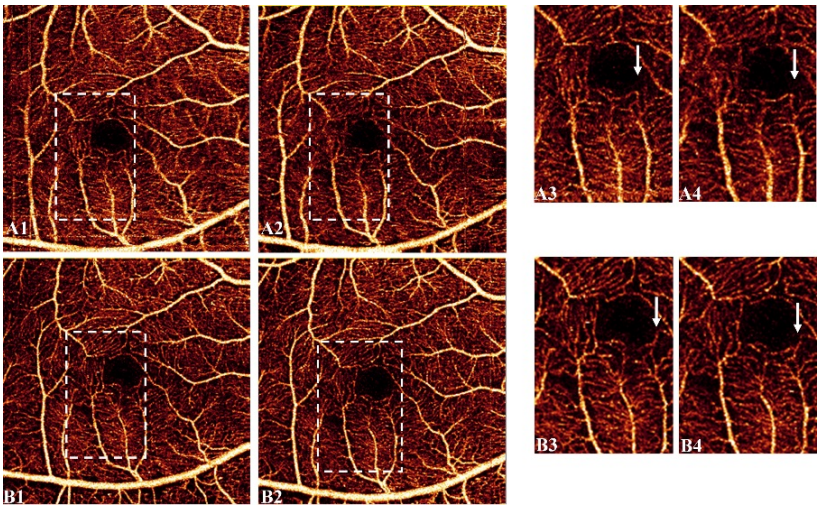

Fig. 5. Similarity of OCTA after MCT for a healthy participant without tracking (A1-A2) and with tracking (B1-B2). Regions enclosed by dashed lines are enlarged in A3, A4 and B3, B4 respectively. Arrows indicate zones where vasculature detail is lost in both MCT-only acquisitions.

4. Discussion

Eradication of motion artifacts in OCTA is critical for accurate interpretation and reliable quantification of clinically relevant parameters. In diabetic retinopathy, residual and distorted lines can complicate detection of key clinical features. Also, high-amplitude pixels contained in line artifacts affect the repeatability of vessel density and non-perfusion area calculation [5, 7]. Retinal vessel density is also relevant in conditions such as type 2 macular telangiectasia [36] and retinal vein occlusion [37]. In AMD, these artifacts introduce inaccuracies to the calculated choroidal neovascularization area, which may be a critical parameter in assessing disease progression. In this work, we have demonstrated that automated software could recognize various types of motion artifacts accurately and that tracking-assisted scanning with MCT could remove motion artifacts more effectively than either method alone.

Two main features allow the MCT algorithm to correct bright line artifacts. The first one is interpolation of the data contained in frames affected by motion, followed by volume registration that corrects eye drift after saccades. The second feature is the weighted merging of registered volumes, which attenuates small motion and improves the SNR. MCT technology was originally developed to eliminate tissue distortions caused by motion in structural OCT. Upon translation to OCTA, MCT continued to utilize the structural OCT information to detect artifacts and determine the transformations to be applied to the angiographic data set. Although the algorithm first removes bright lines caused by microsaccadic motion through merging of the original scans, some residual motion lines remain (Fig. 2(D)). Moreover, inaccuracies in interpolation occasionally cause severe artifacts that we have called distorted lines (Fig. 2(B)). By utilizing the angiographic data in addition

Biomedical Optics EXPRESS

to the structural data as intrinsic indicators of motion, the MCT algorithm may be able to better identify and further reduce these remaining artifacts.

Although tracking-assisted scans do not significantly reduce the total amount of artifacts, the quality of *en face* angiograms was greatly improved by the reduction of bright lines. However, some bright lines do persist, such as the observed in Fig. 3(B1). This is a consequence of the compromise between the tracking system's sensitivity and the scanning time. A disadvantage of tracking-assisted OCTA is that in participants with poor fixation, scanning time becomes unpredictable. In the RTVue-XR system, the tracking sensitivity is relaxed in order to avoid a large number of rescanned frames. This way, the system can restrict the acquisition time by relying on MCT to eliminate small motion artifacts.

Tracking integrated with MCT provided the most effective method to remove motion artifacts. To illustrate the reasons, acquisitions of diabetic patients with tracking (Fig. 6(A1)-6(C1)) and without tracking (Fig. 6(A2)-6(C2)) are shown. Tracking-assisted x/y-fast scans have less bright lines before MCT merging, and remaining lines had smaller width and intensity. As a result, residual lines suppression by weighted merging was more effective (Fig. 4(C)). Furthermore, MCT's volumetric registration feature was also enhanced, as shown by the reduction of distorted lines. Corrupted frames during a microsaccade were ignored in tracking-assisted scanning, which reacquires frames after the eye refocuses on the fixation target, reducing eventual interpolation errors. In contrast, Fig. 6(D2)-6(F2) shows an example of a scan without tracking where strong saccades led to irretrievable sections of a large vessel.

The reduction of stretch artifacts between MCT only and tracking-assisted scanning with MCT was not statistically significant ($p > 0.05$). It was also observed that stretch artifacts were less prevalent in the diabetic group. This may be caused by the algorithm's lower sensitivity due to reduced perfusion, typical of DR. Complete elimination of this peripheral artifact will depend on future improvements of the MCT technology.

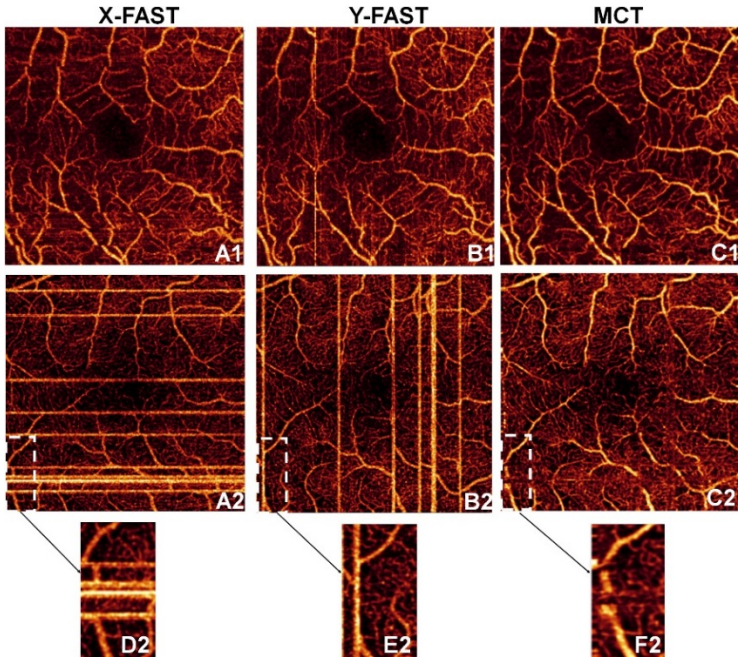

Fig. 6. Benefits of tracking-assisted scanning with MCT, shown by two eyes with DR. Scans of the x-fast, y-fast and MCT are shown with tracking (A1-C1) and without tracking (A2-C2). Angiogram sections with data loss highlighted in A2-C2 are represented in D2-F2.

Biomedical Optics EXPRESS

5. Conclusion

In summary, tracking-assisted scanning integrated with MCT is superior to tracking or MCT alone in removing the total amount of motion artifacts in OCTA. Real-time eye tracking reduces the number and the width of bright-line artifacts in x/y-fast scans. Additionally, the scanning protocol halts the acquisition of frames during saccadic motion. Consequently, fewer residual lines and distorted stripes are observed after MCT registration and merging in the healthy and diabetic groups. The similarity between repeated acquisitions in the same visit was improved by tracking-assisted scanning, as indicated by the larger correlation coefficient between their *en face* OCTA. No conclusive difference in the number of peripheral stretch artifacts was observed between tracking modes.

Funding

National Institutes of Health (NIH) (DP3 DK104397, R01 EY024544, R01 EY023285, P30 EY010572). This work was also supported by unrestricted departmental funding from Research to Prevent Blindness (New York, NY).

Acknowledgments

Technical support and development of DualTrac software: Uday Thummalapalli and Tzu-Yin Wang (Optovue, Inc. Fremont, CA, USA). Miao Zhang and Utkarsh Sharma are employees of Optovue, Inc. Oregon Health & Science University (OHSU), Yali Jia, and David Huang have a significant financial interest in Optovue, Inc. David Huang also has a financial interest in Carl Zeiss Meditec. These potential conflicts of interest have been reviewed and managed by OHSU.